High resolution wind retrieval for SeaWinds

David G. Long and Jeremy B. Luke

Brigham Young University, 459 Clyde Building, Provo, UT 84602, USA

ABSTRACT

The SeaWinds instrument on the QuikSCAT satellite was designed to measure near surface winds over the ocean at a nominal resolution of 25 km with daily global coverage. Recently, reconstruction and resolution enhancement algorithms have been applied to the QuikSCAT measurements to generate high resolution backscatter fields. These high resolution fields make it possible to retrieve the wind at higher spatial resolution. Substantially finer wind and rain features are evident in the dense wind fields. The tradeoff is a higher noise level in the estimated winds. This paper describes the high resolution wind retrieval approach and the accuracy of the resulting high resolution winds. The limitations of the high resolution winds are considered. Methods for improving the accuracy of the data are presented.

Keywords: scatterometer, SeaWinds, radar backscatter, ocean winds, QuikSCAT, wind retrieval, enhanced resolution

1. INTRODUCTION

Currently, two SeaWinds wind scatterometer instruments are flying aboard spacecraft: the first, launched in June 1999, is onboard the QuikSCAT satellite, while the second, launched in December 2002, is aboard the Japanese ADEOS-II satellite. The Ku-band SeaWinds instrument is designed to make nominally 25 km resolution observations of near-surface vector winds over the ocean. The wind measurements are used in weather prediction and in studies of climate and air/sea interaction.[1]

SeaWinds measures the wind over the ocean indirectly: the direct measurement is the normalized radar backscatter (σ°) of the surface, which is related to the wind via a geophysical model function in the wind retrieval process.[2] SeaWinds backscatter measurements are also finding utility in other studies, including sea-ice and iceberg monitoring, melt onset, and vegetation. Such applications are facilitated by applying resolution enhancement and reconstruction techniques[3] to the data. The SeaWinds measurement geometry is well-suited for such applications due to its high azimuth sampling rate, measurement overlap, and dense coverage of the surface.

For previous sensors, resolution enhancement algorithms required multiple passes over the study area. However, the SeaWinds geometry enables estimation of high resolution backscatter fields from only a single pass. More importantly, the estimation can be done separately for forward and aft-facing measurements, though with degraded spatial resolution. Separately estimating the backscatter from different azimuth angles permits retrieval of the wind at very high spatial sampling resolution using conventional wind retrieval algorithms. The tradeoff is a higher noise level in the estimated winds. In this paper we describe the high resolution technique and briefly explore the accuracy of the high resolution winds and their utility in studying mesoscale phenomena. The limitations of the high resolution winds are considered. Section 2 provides background. Section 3 discusses the method for generating high resolution σ° measurements. Section 4 presents the high resolution wind retrieval results and considers the accuracy of the estimated winds. Sample results are presented in Section 5. A summary is provided in Section 6.

Further author information: (Send correspondence to DGL)
DGL: E-mail: long@ee.byu.edu, Telephone: 1 801 422 4383
JBL: E-mail: jbl@et.byu.edu

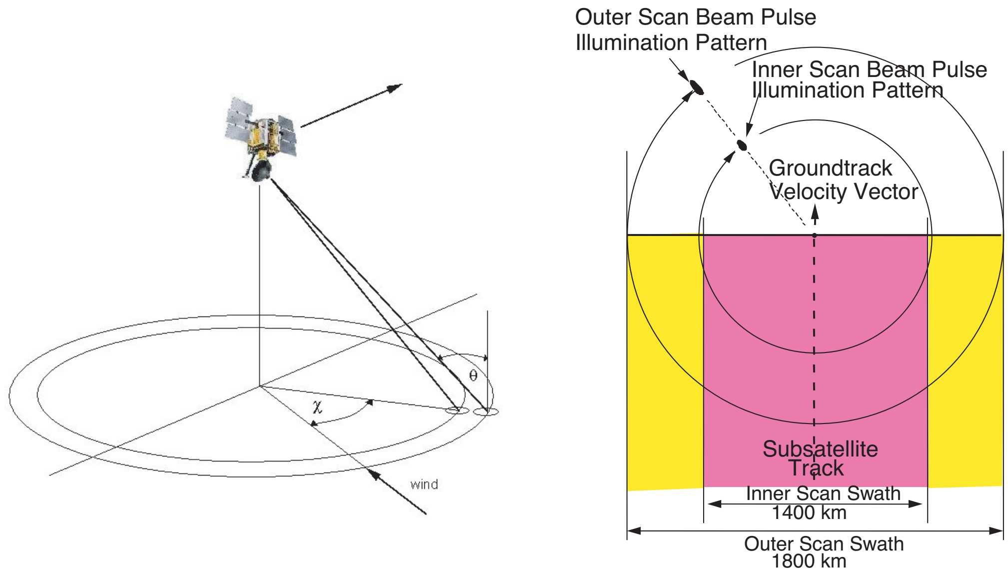

Figure 1. (left) SeaWinds observation geometry. The dual beam antenna spins about nadir. Each beam makes observations at a fixed incidence angle over a range of azimuth angles. (right) Illustration of the SeaWinds observation swath. For a given point within the inner swath σ° measurements at four different azimuth angles, two from each beam, are collected. Only two different azimuth angles are available over the outer swath.

2. BACKGROUND

SeaWinds employs a dual-beam scanning pencil-beam antenna system (see Fig. 1), to make σ° measurements over an 1800 km wide swath at two nominal incidence angles.[4] The inner beam makes horizontally-polarized (HH-pol) σ° measurements at a 46° incidence angle while the outer beam makes vertically-polarized (VV-pol) σ° measurements at a 54.1° incidence angle. Using a chirp modulation and onboard range/Doppler filtering, the antenna beam-limited 25×32 footprint is resolved into eight 6×25 km elements termed 'slices'. The summed slice measurements (which correspond approximately to the beam-limited footprint) are known as 'egg' measurements.[5] Measurements are collected alternately from each beam at a PRF of 180 Hz. The antenna spins at 18 rpm.

Over the inner swath each wvc is observed four times, twice by each beam, once when the beam is looking forward and once when the beam is looking aft as the spacecraft moves along track. Over the outer swath, only two measurements from the outer beam are available. These multiple measurements are at different azimuth angles, an essential requirement for wind retrieval.[2]

To retrieve standard Jet Propulsion Laboratory (JPL) L2B product winds, the egg measurements are first gridded onto a 25 km grid. A given grid element is known as a 'wind vector cell' (wvc). All the σ° measurements whose center falls within a given wvc are used to retrieve the wind for that wvc.

For each wvc, the wind is retrieved with the aid of a geophysical model function (GMF) which relates σ° to the vector wind. The GMF can be written as[6]

$$\sigma^\circ = f(s, \phi - \chi, p, \theta)$$

where s is the wind speed, ϕ is the wind direction relative to north, χ is the look direction of the radar relative to north, p is the polarization of the radar signal (either horizontal or vertical), and θ is the incidence angle of the measurement. The relative azimuth angle between the radar look direction and the wind direction is $\phi - \chi$. Figure 2 illustrates the GMF, plotting σ° versus the relative azimuth angle $(\phi - \chi)$ at several wind speeds for each beam. Note that σ° versus direction is non-unique: several wind directions correspond to the

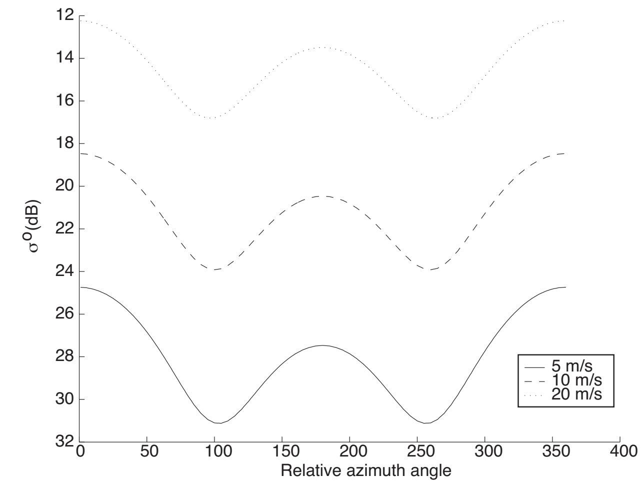

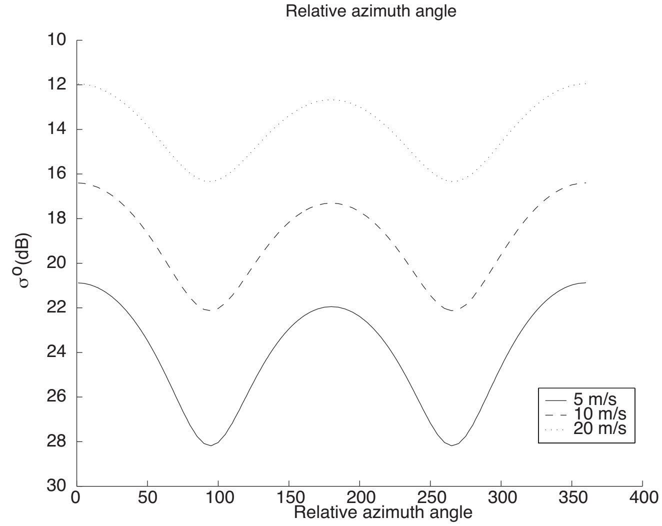

Figure 2. Plots of σ° versus relative azimuth angle $\phi - \chi$ for several wind speeds from the geophysical model function at (left) 46° incidence angle, horizontal polarization, corresponding to the inner beam observations, and (right) 54° incidence angle, vertical polarization, corresponding to outer beam observations.

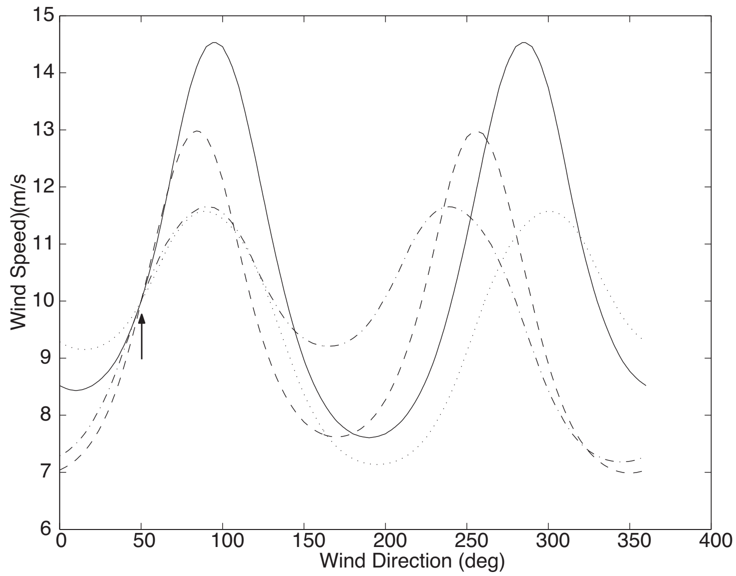

Figure 3. Noise-free wind retrieval illustration. Individual lines represent the possible wind speeds and directions given the observed σ° from each of four colocated σ° measurements taken from different beams. Where they all intersect is the "true" wind speed and direction.

same σ° value. Combining σ° measurements collected at several azimuth angles can ameliorate this problem as illustrated in Fig. 3.

The simple illustration in Fig. 3 becomes more complicated when noisy measurements are considered. Noise shifts the individual curves so they no longer intersect at the same point. To estimate the wind speed and direction, a maximum-likelihood objective function is formulated and optimized, resulting in from one to four wind vector estimates at each wvc.[2] These "ambiguities" have nearly the same wind speed, but differ in direction. To resolve the ambiguity, a separate, post-estimation step is performed. For the standard JPL L2B product, a nudged median-filter based ambiguity selection algorithm is employed which selects a unique wind vector field to ensure spatial consistency in the wind at different wvcs.[7] Though not perfect (heavy rain can contaminate the wind estimates) the resulting wind fields are highly accurate[1,8] and are operationally used for weather prediction.

The standard JPL L2B wind product has a reported resolution of 25 km resolution and is based on the egg measurements. Somewhat higher spatial resolution can be obtained by using slices rather than eggs when gridding the σ° measurements into wvcs; however, the resolution possible from gridding algorithms is limited to the largest dimension of the spatial response function since portions of the spatial response fall outside the grid element.[3] Note that there is a tradeoff between resolution and noise level: low resolution wind estimates tend to have lower noise since they include more averaging. Nevertheless, high resolution wind measurements are sought for applications such as hurricane forecasting, near-shore process studies, and studies of mesoscale wind dynamics.

3. HIGH RESOLUTION σ°

The key to higher resolution wind estimates is enhancing the resolution of the σ° measurements. This is made possible by the dense sampling of the surface by the SeaWinds slice measurements,[5] knowledge of the slice spatial response functions,[5] and reconstruction theory.[3] The slice measurements have significant measurement response overlap. This 'over-sampling', along with the non-ideal roll-off of the spatial measurement response,[3,9] enables a reconstruction algorithm to extract available information from the measurements to produce higher resolution estimates (images) of the surface σ^o, enhancing the effective spatial resolution. The resulting σ° images have finer resolution than the 3 dB resolution of the individual slice measurements. We note that for SeaWinds measurement reconstruction the geometry of the rotating antennas and orientation of the slice measurement response results in variable effective resolution over the swath. Further, while the reconstruction provides improved spatial resolution, its high pass filter characteristics can also enhance the noise in the measurements.

Resolution enhancement algorithms depend on the spatial sampling density of the surface, with finer (denser) sampling resulting in improved resolution. While high spatial sampling density can be achieved by combining multiple passes as done with previous sensors,[3,9] combining multiple passes degrades the temporal resolution and cannot be used for wind retrieval due to the rapid evolution of the wind-driven surface. Further, while land applications can combine the σ° measurements from multiple azimuth angles in the reconstruction process to improve the sampling density,[3,9] wind retrieval requires azimuth diversity. Thus, separate σ° images for the azimuth look directions must be reconstructed to preserve the azimuth diversity of the original measurements.

In this paper the AVE[9] reconstruction algorithm is used. While the AVE algorithm has more limited resolution enhancement capability than the scatterometer image reconstruction (SIR) algorithm typically used for land and ice images, it is also less noisy.[9] The AVE algorithm is used to generate σ° values on a 2.5 km resolution grid for each of the four beam/look direction combinations: h-pol fore and aft azimuth looks and v-pol fore and aft azimuth looks. Over the outer swath only v-pol images are created. Figure 4 illustrates high resolution σ° generated for one orbit (rev) of QuikSCAT. The narrower swath of the H polarization images is apparent.

While specialized skill is required to interpret ocean surface σ° fields, the symmetry and low wind speed central eye of hurricanes make such features easy to identify and track (see Fig. 4). Currently, high resolution σ° fields are being operationally used to support hurricane and severe storm monitoring.[10] Even without wind retrieval, the enhanced resolution σ° fields are a valuable tool in severe storm forecasting. Wind retrieval represents an optimal method for combining the various azimuth looks to further improve the spatial resolution.

4. WIND RETRIEVAL

Wind retrieval requires geometric parameters as well as σ° values. In computing the high resolution σ° fields, the associated incidence and azimuth angles and K_p coefficients are determined. The K_p coefficients describe the variance of the σ° measurements.[2,4] Wind can be retrieved only for the pixels for which multiple σ° values at different azimuth angles are available. Note that while high resolution wind estimates are reported on a 2.5 km grid, the effective resolution of the estimates is coarser than this and varies with swath location.

Given the azimuth and incidence angles and the K_p coefficients at each 2.5 km high resolution wvc, the wind is retrieved separately for each pixel using a standard SeaWinds wind retrieval algorithm. As in conventional wind retrieval, multiple solutions to the maximum-likelihood objective function occur, resulting in from one to four "ambiguities" having similar wind speeds, but with different directions. Associated with each ambiguity is its likelihood value. To select a single ambiguity an initial selection is made by choosing the ambiguity closest (in the vector magnitude difference sense) to the standard JPL L2B 25 km product wind. This ensures that the mean flow exhibited in the high resolution wind field is consistent with the L2B product. A median-filter based ambiguity selection algorithm[11] with a window size of 17.5 km $\times$ 17.5 km is then applied to select the final ambiguities. A variety of window sizes were evaluated, and this size was adopted as providing the best subjective tradeoff between computation and performance.

To evaluate the accuracy of the high resolution wind field estimates, simulation is employed. Unfortunately, maximum-likelihood wind retrieval is only asymtoticly unbiased,[12] and estimate bias becomes important as the resolution is enhanced. To minimize the bias in the final product, the bias in the retrieval algorithm is estimated and removed from the retrieved winds. Simulations are employed to estimate the bias as a function of wind direction and speed at each cross-track location. The resulting errors are binned according to the estimated wind direction and speed and averaged. The average bias is then removed from the retrieved winds. Separate simulations show that corrected winds exhibit little bias. Figure 5 shows the root-mean-square (RMS)

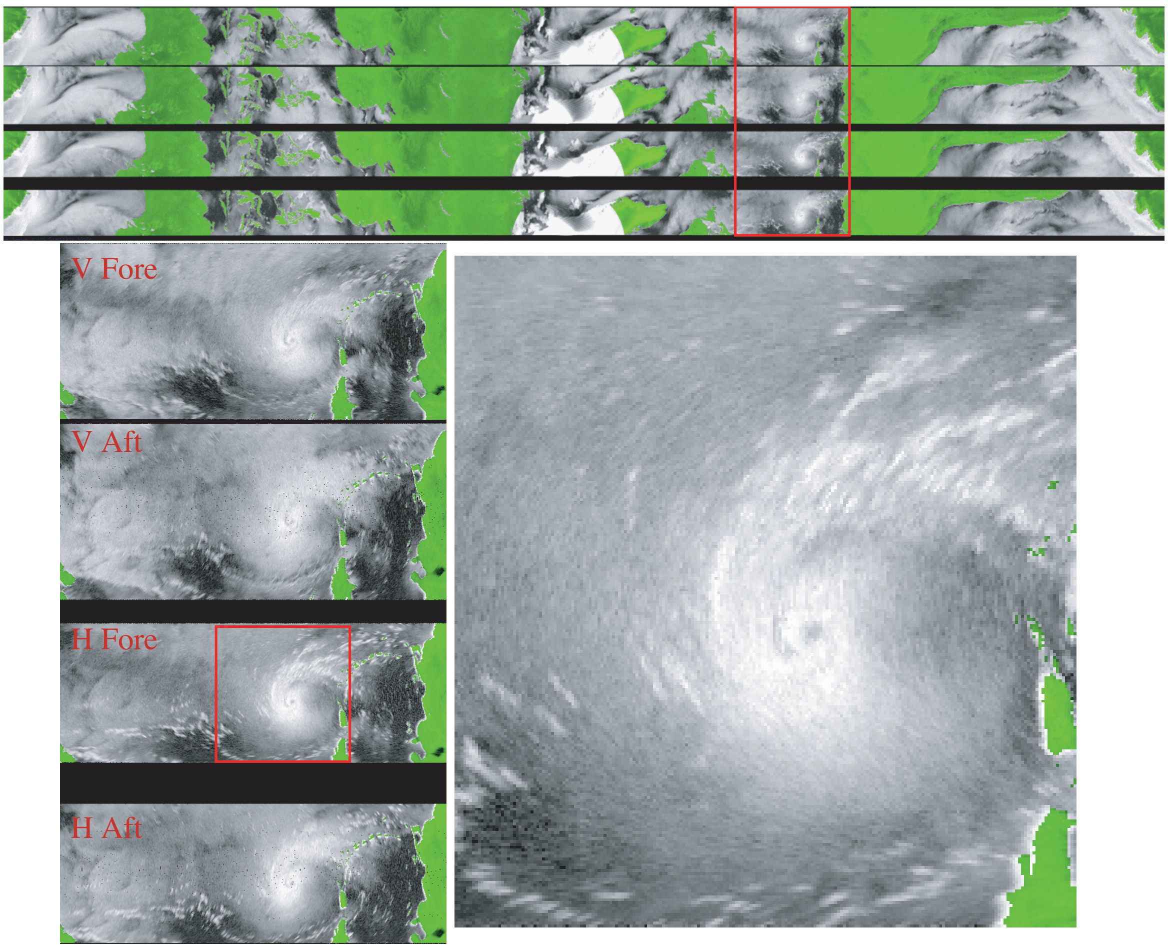

Figure 4. AVE-derived 2.5 km pixel resolution σ° (in dB) fields for SeaWinds derived from rev 1201 (14 Jul. 1999). (top panel) σ° images from the full orbit from the southern-most point, over the equator and northern hemisphere, and back over Antarctica from left to right in a space-based mercator (satellite swath) projection. Within this panel from top to bottom the sub images are Forward-look, V-pol; Aft-look, V-pol; Forward-look, H-pol; Aft-look, H-pol. (left panel) A closer view of the boxed area in the top panel, east of Central America. (right panel) Expanded view of the boxed area in the aft-look, H-pol image in the left panel over Hurricane Floyd. The central eye is visible as a darker spot near the image center. The island of Puerto Rico is to the right (south) of the hurricane eye. Texturing in the image is the result of of mesoscale wind variability and noise. Some of the small, bright features may be due to enhancement of the backscatter due to rain. The corresponding high resolution wind fields in Fig. 6 tend to re-enforce this observation. The greyscale for σ° is -30 to 0 dB, corresponding to from black to white.

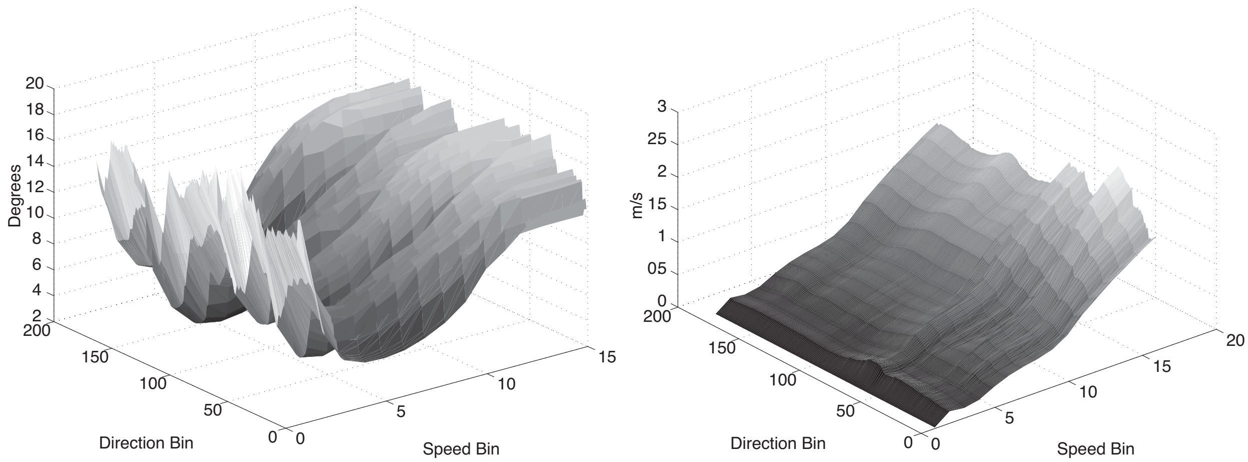

Figure 5. RMS wind error binned by the true wind computed via simulation for high resolution wind estimation. (left) Direction error. (right) Speed error. Simulations are conducted by randomly choosing a 'true' wind within each 2 deg by 1 m/s bin and retrieving the wind. Monte Carlo noise is added to the σ° values computed using the GMF and realistic geometry parameters. The error is the difference between the true wind and the ambiguity closest to the true wind vector. The RMS of 200 realizations for each bin is shown.

error of the bias-corrected wind estimates as a function of swath location and true wind speed and direction. As expected the high resolution winds are noisier than conventional 25 km L2B product winds. This can be ameliorated by spatial averaging, at a cost of degraded spatial resolution.

Figure 6 compares high resolution and conventional winds estimated over Hurricane Floyd, corresponding to Fig. 4. The improvement in spatial resolution of the wind estimates is clear and it is possible to resolve the hurricane eye in the high resolution wind speed image, something not possible in the low resolution wind speed image. Some of the detail in the wind speed image can be attributed to the effects of rain on the backscatter. Rain tends to attenuate high wind speeds, while enhancing low wind speeds.

While L2B wind estimates are not available near coasts, high resolution winds are retrieved right up to the coastline in order to support near-coastal studies. However, caution is suggested when using near-land high resolution winds since they may be land contaminated. The contamination occurs since land σ° values are often much larger than ocean σ° and can contaminate a nearby ocean measurement via the sidelobes of the spatial response function.

Validation of the high resolution wind fields is difficult due to the lack of suitable comparison data. The high resolution wind fields compare very well with conventional L2B winds. Comparison of high resolution estimated winds with buoy measurements and SAR-estimated wind fields is most encouraging. We conclude that with care, the high resolution measurements are suitable for near-coastal studies, monitoring severe weather events, and studying mesoscale variability.

5. CONCLUSION

Though originally designed to measure vector winds over the ocean at 25 km resolution, SeaWinds can retrieve vector winds at higher resolution, albeit with reduced accuracy since the enhanced resolution high resolution σ° values are noisier than the egg σ° values conventionally used to retrieve the wind. The high resolution winds are not suitable for all applications due to the high noise level and the temporal sampling. However, they can be applied in the study of near-coastal and mesoscale winds. A bias correction step and improved ambiguity selection increases the wind accuracy. Validation of the high resolution wind estimates is continuing and comparison against SAR images and other wind sensors is encouraging. Operational production of high resolution winds in order to support hurricane and severe storm monitoring was recently initiated.

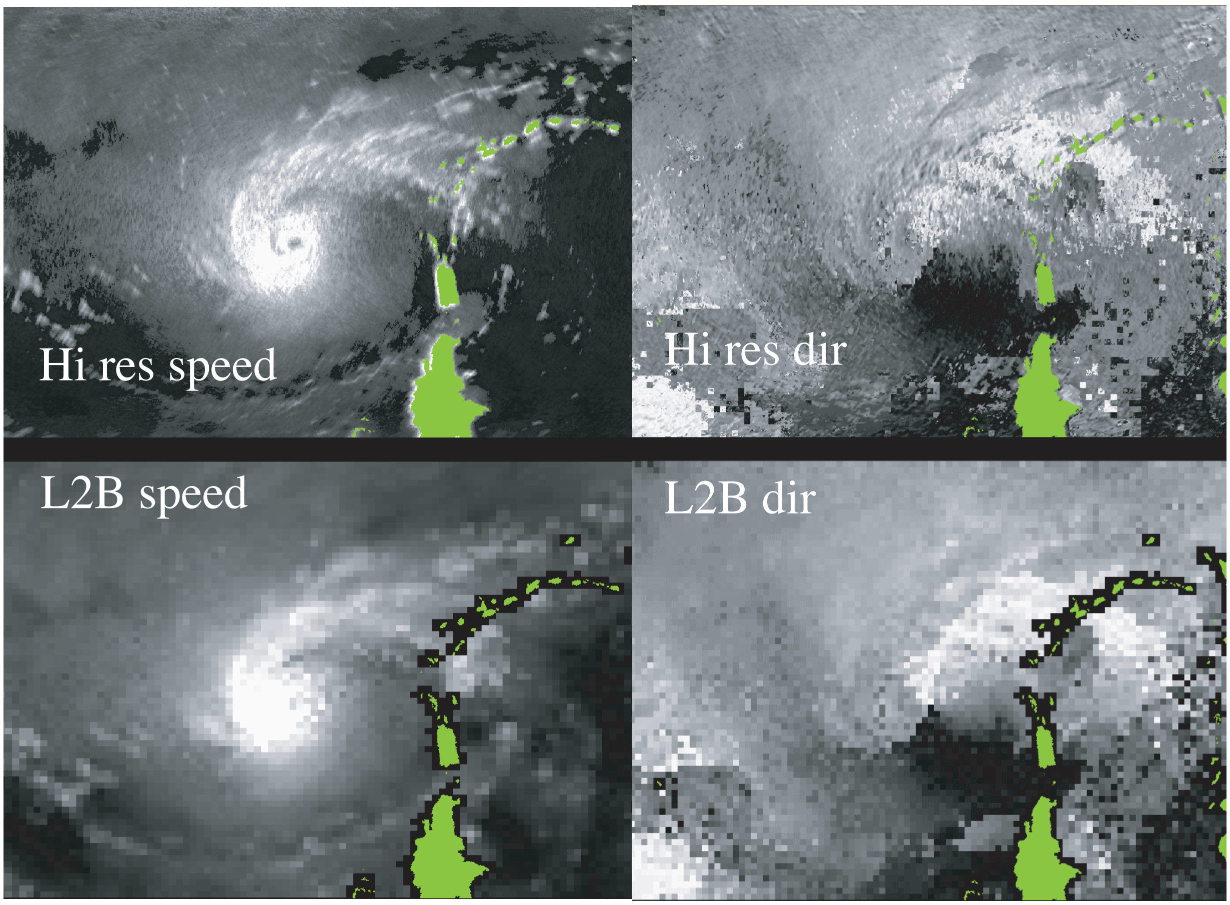

Figure 6. Winds derived from high resolution σ° data from QuikSCAT rev 1201 (14 Jul. 1999). Compare Fig. 4. (top, left) High resolution (2.5 km/pixel) wind speed. (bottom, left) Low resolution (25 km) wind speed from the standard L2B product. (top, right) High resolution wind direction. (bottom, right) Low resolution (25 km) wind direction. Wind speeds from 0 to 25 m/s correspond to from black to white, while wind directions from 0 to 180 to 360 correspond to from white to black to white. The low wind speed eye of Hurricane Floyd is clearly visible in the high resolution wind field, but cannot be resolved in the low resolution wind field.

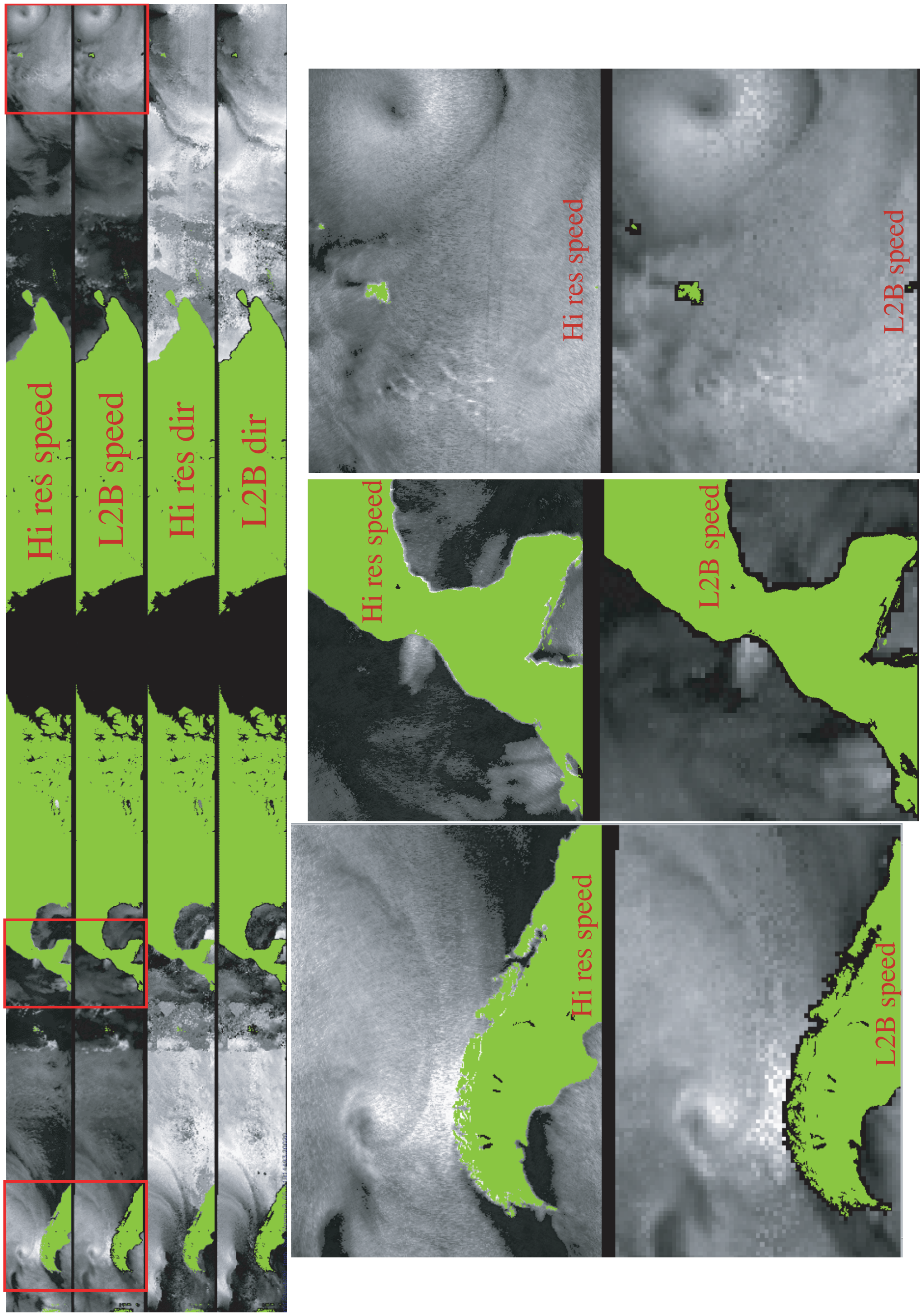

Figure 7. Additional examples of high resolution wind retrieval from QuikSCAT rev 14436 (28 Mar. 2002). (left panel) Winds retrieved over most of an orbit, comparing high and low resolution wind estimates. (right panels) Expanded views of selected boxed areas. The top panel shows a depression in the southern Indian ocean. The center panel shows high winds blowing through a pass in southern Mexico. The lower panel shows a cyclone off the western coast of South America.

ACKNOWLEDGMENTS

This work was funded as part of the Ocean Vector Winds Science Team. SeaWinds data was obtained from the Physical Oceanography Distributed Data Archive (PO.DAAC) at the CalTech Jet Propulsion Laboratory.

REFERENCES

1. W. Liu, "Progress in scatterometer application," *J. Oceanogr.* **58**, pp. 121–136, 2002.
2. F. Naderi, M. Freilich, and D. Long, "Spaceborne radar measurement of wind velocity over the ocean–an overview of the NSCAT scatterometer system," *Proc. IEEE* **79**(6), pp. 850–866, 1991.
3. D. Early and D. Long, "Image reconstruction and enhanced resolution imaging from irregular samples," *IEEE Trans. Geosci. Remote Sens.* **39**(2), pp. 291–302, 2001.
4. M. Spencer, C. Wu, and D. Long, "Improved resolution backscatter measurements with the SeaWinds pencil-beam scatterometer," *IEEE Trans. Geosci. Remote Sens.* **38**(1), pp. 89–104, 2000.
5. I. Ashcraft and D. Long, "The spatial response function of SeaWinds backscatter measurements," in *Earth Observing Systems IV*, W. L. Barnes, ed., *Proc. SPIE* **to appear**, 2003.
6. F. J. Wentz and D. K. Smith, "A model function for the ocean-normalized radar cross section at 14 GHz derived from NSCAT observations," *J. Geophys. Res.* **104**, pp. 11,499–11,514, May 1999.
7. B. W. Stiles, B. D. Pollard, and R. S. Dunbar, "Direction interval retrieval with thresholded nudging: A method for improving the accuracy of QuikSCAT winds," *IEEE Trans. Geosci. Rem. Sens.* **40**, pp. 79–89, 2002.
8. D. Draper and D. Long, "An assessment of SeaWinds on QuikSCAT wind retrieval," *J. Geophysical Res.* **107**(C12), pp. 3212–3226, 2002.
9. D. Long, P. Hardin, and P. Whiting, "Resolution enhancement of spaceborne scatterometer data," *IEEE Trans. Geosci. Remote Sens.* **31**(3), pp. 700–715, 1993.
10. D. Long, "High resolution wind retrieval from SeaWinds," *Proc. IGARSS 2001* , pp. 2187–2189, 2001.
11. S. Shaffer, R. Dunbar, S. Hsiao, and D. Long, "A median-filter-based ambiguity removal algorithm for NSCAT," *IEEE Trans. Geosci. Remote Sens.* **29**(1), pp. 167–174, 1991.
12. T. Oliphant and D. Long, "Accuracy of scatterometer-derived winds using the Cramer-Rao bound," *IEEE Trans. Geosci. Remote Sens.* **37**(6), pp. 2642–2652, 1999.